

## Influence of helically shaped fields on particle transport in the RFP

I. Predebon<sup>1</sup>, L. Marrelli<sup>1</sup>, P. Martin<sup>1</sup> and R.B. White<sup>2</sup>

<sup>1</sup> *Consorzio RFX, Associazione Euratom-Enea sulla fusione, Padova, Italy*

<sup>2</sup> *Princeton Plasma Physics Laboratory, Princeton, NJ, USA*

Due to its peculiar  $q$  profile, the Reversed Field Pinch (RFP) configuration is characterized by a wide spectrum of  $(m, n)$  resonant tearing modes (Multiple Helicity, MH regime) whose amplitude is such that typically magnetic surface destruction occurs in the plasma core [1]. On the contrary, theory predicts the existence of Single Helicity (SH) plasmas [2], sustained by a dynamo mechanism based on an individual  $m = 1$  resistive instability and characterized by helical closed magnetic surfaces. Particle orbits and transport in SH regimes are numerically investigated with the guiding center code ORBIT [3]. The study is based on the RFX geometry ( $R = 2$  m,  $a = 0.46$  m), and in particular the 2<sup>nd</sup> order Shafranov equilibrium is built from experimental values of magnetic field at the edge and plasma current (shot #13250), by means of the  $\mu&p$  model. The single perturbation  $(m, n) = (1, 8)$  is computed solving the Newcomb equation, and for the present analysis has a peak value  $\max(b_r)/B_{\text{axis}} \sim 3.5\%$ . In the following we adopt the poloidal flux  $\psi_p$ , the poloidal and toroidal angles  $\theta$  and  $\zeta$  as flux coordinates [3].

### Collisionless particle orbits

The helical field enriches the trajectory typologies, in comparison with an axisymmetric RFP [4]. This is due to the fact that the field has two types of ripples: the variation of  $|B|$  corresponds to the superimposition of a toroidal ripple (slow sinusoidal variation) and a helical ripple (faster variation), as shown in Fig. 1. Trapped particles can be either localized or blocked, depending on the initial position and pitch, and on the perturbation strength. *Localized particles* (trapped in the helical ripple), with high magnetic moment  $\mu = mv_{\perp}^2/2B$ , execute thin banana orbits (the ion banana width is  $\sim 1$  mm for a thermal

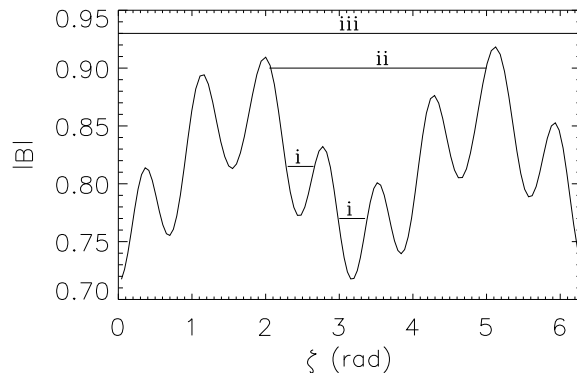


**Figure 1:** Magnetic field ripple (initial  $\psi_p = 0.04$ ) with the three trapping states: localized (i), blocked (ii) and passing (iii).



The present work deals with monoenergetic test particles at the background plasma temperature, with energy conserving collisions. Simulations carried out for different values of the energy have confirmed that the choice of the background temperature properly describes particle confinement of a Maxwellian energy distribution with a full energy-exchange collision operator [6].

The transport properties are deduced computing the loss time  $\tau_L$  a set of particles takes to exit from a preassigned region, bounded by a  $\psi_p = \text{const}$  surface. For the present analysis the particles are deposited along the curve  $(\psi_p, \theta) = (0.025, 0)$ , with uniform pitch angle distribution in the interval  $[-1, +1]$ ; the loss border is located at  $\psi_p = 0.060$ .

As already mentioned, pitch angle scattering turns out to be more important than the classical one. The blue and green curves in Fig. 3 show, at the O-point, a ratio between classical scattering loss time and pitch angle scattering loss time  $\tau_L^c/\tau_L^p \sim 3.5$ , both for ions and electrons.

The application of both collisional mechanisms (full scattering operator) further increases radial transport (red lines),  $1/\tau_L^f \sim 1/\tau_L^c + 1/\tau_L^p$ . In this case the ratio between electron and ion loss times is  $\tau_{Le}^f/\tau_{Li}^f \sim 20$ . Concerning classical scattering, it is worth noting that  $\tau_{Le}^c/\tau_{Li}^c < (M/m)^{1/2}$  due to the presence of toroidal and helical drifts.

### Helical electrostatic potentials

The introduction of a helical electrostatic potential makes the thermal particle transport ambipolar. Such a potential is analytically built in a small island approximation, so that magnetic and equipotential surfaces coincide (thus the island is smaller than that of Fig. 2). We adopt for the potential a linear dependence on the perturbed helical flux,  $V(\psi_h) = k_{\text{SEP}}(\psi_h/2\psi_1) + \text{const}$  with  $\psi_h(\psi_p, \theta, \zeta) = \psi_{h0}(\psi_p) - \psi_1 \cos(m\theta - n\zeta)$  and  $k_{\text{SEP}}$  potential between O-point and separatrix of the island;  $\psi_{h0}(\psi_p) = (n/m)\psi(\psi_p) - \psi_p$  is the unperturbed helical flux and  $\psi_1$  is the perturbation amplitude. The value of the perturbation is given by  $\psi_1 = -q'(n/m)(w^2/16)$ , with  $q' = dq/d\psi_p$  calculated at the tearing mode resonance and  $w$  island width. For a poten-

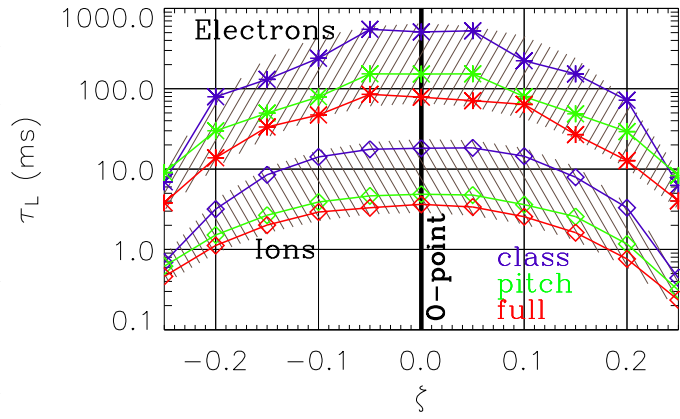


**Figure 3:** Loss time versus toroidal angle for ions and electrons, with classical (blue lines), pitch angle (green) or both (red) the collision operators turned on.

tial between 0-point and separatrix  $k_{\text{SEP}} \sim 100$  eV the two loss curves cross each other. Even though the  $\vec{E} \times \vec{B}$  component perpendicular to the surfaces vanishes, the potential provides quasi-neutrality acting on the particle drifts.

The ambipolar transport is dominated by the slowest species, electrons in this case. At the O-point we find  $\tau_{L \text{ amb}} \sim \tau_{L e}/2$ . If we define an effective diffusion coefficient  $D \propto (\Delta r)^2/2\tau_{L \text{ amb}}$ , so to compare particle confinement in SH and MH, we find a value,  $D \sim 0.15 \text{ m}^2/\text{sec}$ , two orders of magnitude lower than MH diffusivity in the core, see [7] for an example.

In order to estimate the effect of the island on the temperature of ions and electrons, transport properties of high energy particles interacting with the bulk-balancing ambipolar potential have been studied. For a particle energy

$3T_{\text{th}} \lesssim T \lesssim 6T_{\text{th}}$  electrons are much better confined than ions: almost one order of magnitude difference in loss time is found in this temperature range, as shown in Fig. 4-b, which suggests an increased electron temperature within the helical structure.

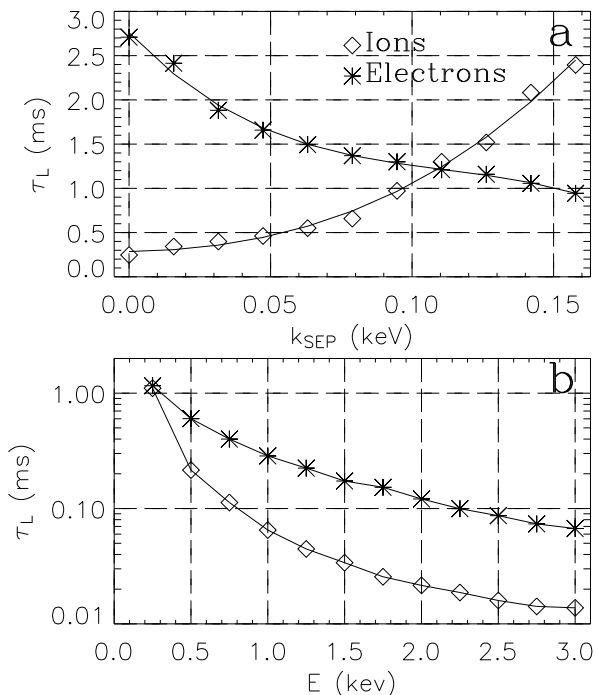


**Figure 4:** Effect of the helical potential on thermal particles (250 eV). The two loss-curves cross each other for a potential  $\sim 100$  eV (a). For this ambipolar potential, superthermal electrons are better confined than superthermal ions (b).

## References

- [1] D'Angelo F. and Paccagnella R., Phys. Plasmas **3**, 2353 (1996).
- [2] Cappello S. and Paccagnella R., Phys. Fluids B **4**, 611 (1992).
- [3] White R.B. and Chance M.S., Phys. Fluids **27**, 2455 (1984).
- [4] Wakatani M. and Itatani R., J. Phys. Soc. Japan **34**, 181 (1973).
- [5] Mynick H.E., Phys. Fluids **26**, 1008 (1983).
- [6] Boozer A.H., Kuo-Petravich G., Phys. Fluids **24**, 851 (1981).
- [7] Gregoratto D. *et al*, Nucl. Fus. **38**, 1199 (1998).